ON THE RELATIONSHIP BETWEEN BRIGHTNESS TEMPERATURE AND THUNDERSTORM EVOLUTION

A Senior Honors Thesis

By

ANITA DENISE RAPP

Submitted to the Office of Honors Programs
& Academic Scholarships
Texas A&M University
In partial fulfillment of the requirements of the

UNIVERSITY UNDERGRADUATE
RESEARCH FELLOWS

April 2000

Group: Physical Sciences

ON THE RELATIONSHIP BETWEEN BRIGHTNESS TEMPERATURE AND THUNDERSTORM EVOLUTION

A Senior Honors Thesis

By

ANITA DENISE RAPP

Submitted to the Office of Honors Programs
& Academic Scholarships
Texas A&M University
In partial fulfillment of the requirements of the

UNIVERSITY UNDERGRADUATE
RESEARCH FELLOWS

Approved as to style and content by:

Michael I. Biggerstaff

Edward A. Funkhouser

April 2000

Group: Physical Sciences

ABSTRACT

On the Relationship Between Brightness Temperature

and Thunderstorm Evolution

Research Fellows: (April 2000)

Anita Denise Rapp
Department of Atmospheric Sciences
Texas A&M University

Fellows Advisor: Dr. Michael I. Biggerstaff
Department of Atmospheric Sciences

The impact of tropical precipitation on the global energy budget has long been an important topic of investigation. To more accurately assess large-scale heating, we must first understand the small scale cloud processes that make up tropical precipitation. In particular, we must relate observations obtained from remote sensing platforms, such as satellites, to the physical properties of clouds. This research aids that goal by relating microwave signatures observed in convective clouds to the cloud's stage of evolution, as diagnosed using weather radar. By studying the brightness temperature at four different frequencies, 10.7 GHz, 19.35 GHz, 37.1 GHz, and 85.5 GHz, throughout the life cycle of a convective cell, we are better able to document the evolution of the differing amounts and combinations of liquid and frozen hydrometeors. This is key to understanding the cloud's radiative processes and precipitation production. The data will be taken from the National Aeronautics and Space Administration Tropical Rainfall Measuring Mission Kwajalein Experiment. Reflectivity data from the Kwajalein radar and brightness

temperature data from the Advanced Microwave Precipitation Radiometer will be used to investigate a storm system that was sampled continuously from 0056-0214 UTC on 29 August 1999. This continuous data set offers an opportunity to evaluate the relationship between brightness temperature and thunderstorm evolution within tropical convective systems.

Analysis of the convective cells within this system shows that proper interpretation of measured brightness temperatures requires knowledge of the thunderstorm evolution. In particular, the combination of low 85 GHz brightness temperature with moderately strong 10 GHz brightness temperatures was found to be associated with dissipating convective cells. These results show that the study of convective cell evolution is an important part in understanding cloud radiative processes.

Acknowledgements

Special thanks are due to Dr. Michael I. Biggerstaff for his valuable input and guidance. I am grateful to the members of the Mesogroup, especially Eun-Kyoung Seo, Gordon Carrie, Roberto Gasparini and Jason Jordan, for their help and support. Thanks are also due to my parents, Robert and Cathy Rapp, for their encouragement. This research is in support of the National Aeronautics and Space Administration Tropical Rainfall Measuring Mission [NAG5-4776].

TABLE OF CONTENTS

LIST OF FIGURES

On the Relationship Between Brightness Temperature and Thunderstorm Evolution

Introduction

The impact of tropical precipitation on the global energy budget has long been a topic of investigation. Riehl and Malkus (1958) determined that latent heat released in tropical convection provided the balance of poleward transport of energy. Further studies (Yanai, 1973) described the impact of tropical convection on large-scale flow. Yanai described the effects of tropical convection on the larger-scale environment as an apparent heat source, Q_1, and an apparent moisture sink, Q_2, both of which are associated with condensation of water vapor to produce rainfall. For the purposes of this study, only the apparent heat source, Q_1, will be discussed. The apparent heat source is described by the following equation:

$$\underset{(a)}{Q_1} = \underset{(b)}{Q_R + L_v(c-e)} - \underset{(c)}{(\partial/\partial p)\overline{s'\omega'}} \qquad (1)$$

where Q_R is the heating due to radiation, L_v is the latent heat of condensation, c is rate of condensation, e is rate of evaporation of cloud droplets and precipitation, p is pressure, s' is the deviation of dry static energy from a horizontal average, ω' is the deviation of vertical velocity from a horizontal average. The last term (c) represents the vertical flux convergence of energy by the updrafts and downdrafts within clouds. Both term (a) and term (c) are typically small in comparison with term (b) as noted by Houze (1982). If

This thesis follows the style and format of the *Journal of the Atmospheric Sciences*.

term (b) is integrated vertically from the ground to the top of the cloud, the net condensation minus evaporation is simply the rainfall from the cloud system. Rainfall can be measured. Hence, measurements of rainfall can be equated to the value of vertically integrated heating.

Unfortunately, it is not only the amount of heating, but also the vertical level of maximum heating that is important. For example, Hartmann et al. (1984) and DeMaria (1985), showed that the vertical profile of heat release determines the mode of large-scale circulations in the Earth's atmosphere.

While rainfall can be directly measured over land using gauges, there are few landmasses in the tropical latitudes. Obtaining direct rainfall measurements over the open ocean is impractical. Fortunately Wilheit et al. (1977) derived a way to estimate rainfall from satellite-based measurements of the amount of radiation being emitted from a cloud system. The radiation is often measured in terms of brightness temperature. This allows a space-based remote sensing platform to be used to obtain estimates of rainfall over the tropics.

The Tropical Rainfall Measuring Mission, TRMM, is a NASA satellite-based project to determine the distribution and variability of precipitation and latent-heat release in the tropics (Simpson et al. 1988). The TRMM satellite was launched from Japan in 1997. Because precipitation emits radiation at microwave frequencies, the satellite is equipped with a radiometer to measure the upwelling radiation produced by tropical convection. The TRMM satellite has a large field-of-view, so images of precipitation appear "smeared" because of the low resolution of the radiometer. It is important to

related these "smeared" observations as seen through the satellite's field-of-view to the physical properties within tropical convection. TRMM does this through a network of ground-validation sites. The ground-validation sites, such as the one in Kwajalein, Marshall Islands, are equipped with weather radars and a network of rain gauges to aid in relating the small-scale measurements to those observed by the satellite. This study will utilize data collected from the ground-based radar on Kwajalein, during a special field campaign in which an instrumented aircraft equipped with a TRMM-like radiometer flew over tropical convection. This combination of radar and aircraft data will be used to examine the relationship between upwelling radiation (brightness temperature) from convective clouds to the stage of the cloud's life cycle.

By examining the small-scale processes associated with an individual cloud's evolution, we hope to improve the interpretation of brightness temperatures observed by the TRMM satellite. For example, brightness temperature is a function of total liquid water and ice amounts, as well as the vertical distributions and sizes of the hydrometeors within the cloud (Adler et al. 1991; Smith et al. 1992). The hydrometeor distributions can also be related to the vertical profile of heating within the cloud (Olson et al. 1999). Hence, by improving the interpretation of brightness temperatures we can improve the retrieval of the vertical distribution of heating from precipitation. This will aid in forecasting large-scale circulations like El Niño and La Niña.

The goal of this study is to analyze data collected during the Kwajalein Experiment, KWAJEX, to establish the relationships between brightness temperature and thunderstorm evolution. Simultaneous data collected by ground-based radar and by an

airborne radiometer from 0056-0214 UTC on 29 August 1999, offer an opportunity to investigate this relationship. This system was sampled from an intense line of convection until almost complete dissipation. Related studies have looked at the relationships between brightness temperature and tropical convection (e.g. McGaughey et al. 1996; McGaughey and Zipser 1996; Lui and Curry 1998; Viltard et al. 1998), however, a continuous data set throughout almost the entire life cycle of a convective system has not been collected previously. This study provides a unique analysis of how brightness temperature varies over the life cycle of convection.

Results from this study showed that the changes in brightness temperature and radar reflectivity structure are consistent with the conceptual model of thunderstorm evolution. In particular, the presence of large ice particles above moderate rainfall in dissipating convection leads to a depression in 85 GHz brightness temperatures with only moderately intense 10 GHz brightness temperatures. This combination of brightness temperatures has been observed previously but poorly understood.

By evaluating this relationship, the current study improves retrieval of the hydrometeor profiles within tropical convective systems from which the vertical heating profiles are derived.

Data

The data for this research was collected during the National Aeronautics and Space Administration Tropical Rainfall Measuring Mission (TRMM) Kwajalein Experiment (KWAJEX). KWAJEX, took place from 23 July 1999 to 16 September 1999. The data specifically used in this project was taken from a convective system that occurred on 29 August 1999. The system was sampled continuously from an intense convective line to a broad stratiform (horizontally uniform rain) region. The hours of 0056 UTC to 0214 UTC have been analyzed for this project.

The radar data was collected from the Kwajalein S-band Doppler radar operated by Aeromet. The Kwajalein radar is located at 8.72°N, 167.73°E, and has a wavelength of 10.71 centimeters, a beamwidth of 1.12°, and a pulse duration of 0.72 microseconds. Only the reflectivity data were used. Reflectivity (Z) is a measure of the sum of the precipitation particles diameters to the sixth power. Large particles produce high reflectivity values. Given that the value of reflectivity covers many orders of magnitude, the reflectivity is often given using a logarithmic scale and denoted by dBZ.

The airborne microwave radiometer data used in the analysis was collected by the Advanced Microwave Precipitation Radiometer, AMPR, which was mounted on the NASA DC-8 aircraft. The AMPR is an airborne, four-frequency, 10.7 GHz, 19.35 GHz, 37.1 GHz, 85.5 GHz, scanning microwave radiometer. The reflector scans a total of 90° (±45° from nadir) and samples 50 beam spots every 1.8° angle (Spencer et al. 1994).

For the convective system on 29 August 1999, the DC-8 flew at an altitude of approximately 12.5 kilometers along and on the backside of a line of convection. The DC-8 flew this line fourteen times as the system propagated across the Kwajalein radar domain.

The Conceptual Model of a Thunderstorm

A thorough discussion of thunderstorms and the processes that affect their growth and decay is essential to the understanding of this research. There are a number of environmental conditions that can affect the development and evolution of a thunderstorm. For simplicity, the conceptual model of a single-cell storm will be considered (Figure 1). The multicellular thunderstorm can be thought of as a cluster of single cells.

The life cycle of a single-cell thunderstorm can be described in terms of three stages: developing, mature, and dissipating (Byers and Braham 1949). The developing stage consists of a single updraft. As the unstable air parcel rises through the troposphere, water vapor condenses and precipitation particles form. Initially the cloud contains mostly rain drops with very little ice. When these particles grow large enough, the particle fallspeeds will overcome the updraft speed. This helps initiate the downdraft. Entrainment of dry environmental air into the saturated downdraft causes evaporation and cooling. This increases the negative buoyancy and enhances the downdraft. The formation of a downdraft indicates that the cell has reached the mature stage.

In the mature stage, a thunderstorm has both an updraft and a downdraft. The rain drops carried aloft have had time to freeze into a variety of ice particles. Hence, during the mature stage, large ice particles can be found over heavy rainfall. When the outflow from the rainfall-driven downdraft reaches the surface and spreads, it begins

cutting off the unstable air feeding the updraft and the updraft begins to weaken. This results in a weaker downdraft also.

The dissipating stage of a thunderstorm usually consists of a weak updraft in the upper levels of the cloud, as well as a weakening downdraft from mid-to-low levels of the cloud. Since the updraft has weakened and since most of the rain has already fallen to the surface, the dissipating stage is marked by smaller rain rates and a smaller number of large ice particles aloft.

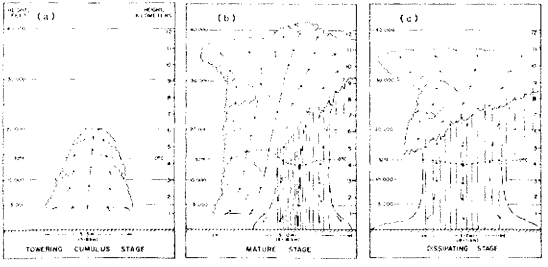

Figure 1. (a) The towering cumulus stage, (b) mature stage, and (c) dissipating stage of a short-lived convective cell. (Weisman and Klemp, 1986. Courtesy of C.A. Doswell, NOAA/ERL/WRP, Boulder, CO.; adapted from Byers and Braham, 1949.)

Brightness Temperature Overview

Before further analysis, it is important to understand what brightness temperature measures. Brightness temperature, T_B, is described by application of Rayleigh-Jean's approximation to the Planck radiation function (2).

$$T_B = B_\lambda \lambda^4 / 2kc \qquad (2)$$

T_B is the object's brightness temperature, λ is the wavelength of emitted radiation, B_λ is the amount of radiation emitted at that wavelength (related to the object's temperature and its ability to radiate at that wavelength), k is the Boltzmann constant, and c is the speed of light. This simplified form of Planck's law shows that brightness temperature is a function of wavelength and the amount of energy the object emits at that wavelength.

A radiometer measures the amount of radiation received at the instrument as a function of wavelength. A satellite radiometer pointing downward would sense radiation from the entire vertical column below it. So brightness temperature, as measured by a satellite-based radiometer, is a vertically integrated quantity. In the case of precipitation, the radiometer measures the upwelling radiation from all the hydrometeors within the vertical column. This is very important for remote sensing applications and can help in identifying hydrometeors within convective storms.

To interpret brightness temperature observations, a cold, uniform background is required. Land surfaces have large variability in emissivity (the ability to radiate at a particular wavelength) which makes it difficult to interpret brightness temperature observations. The ocean surface is an ideal background because it is uniform and has a

low emissivity at microwave frequencies (Wilheit, 1986). Emission from cloud and rain water appear warm against the radiometrically cold ocean surface.

The four different channels (10.7, 19.35, 37.1, and 85.5 GHz) on the Advanced Microwave Precipitation Radiometer (AMPR), identical to those of the TRMM Microwave Imager, are sensitive to different processes within the storm cell. The 10.7 GHz channel is sensitive to emission from rain. The 19.35 GHz channel has a much greater sensitivity to rainwater, but the signal tends to saturate in cells with high rain intensities. The 37.1 GHz channel has an even higher sensitivity to rainwater, but is also sensitive to cloud water. This makes it more difficult to distinguish how much of the signal is due to cloud water versus rainwater emission. At 37.1 GHz evidence can be seen of scattering of upwelling radiation by large ice hydrometeors within the storm cell. Scattering by ice hydrometeors results in a depression in brightness temperature because the upwelling radiation gets redirected away from the viewing angle of the radiometer. Finally, the 85.5 GHz channel brightness temperatures are dominated by ice scattering (Wilheit et al. 1982). However, the brightness temperature depression due to large ice scatterers can be masked by the presence of supercooled water. Supercooled water will absorb the radiation being scattered by the ice and re-emit it.

Using a combination of all these frequencies, the idealized set of brightness temperatures associated with distributions of hydrometeors within the conceptual model of a single-cell thunderstorm can be presented. During the developing stage, the idealized storm will consist mostly of rain and cloud water with very little ice. Hence, there will be an increase in brightness temperature at 10.7 and 19.35 GHz with saturation at 19.35

GHz for heavy rain cores. The 37.1 GHz channel will show some warming relative to the ocean background, but there will be no scattering signature here or at 85.5 GHz. During the mature stage, the idealized storm will have warm 10.7 and 19.35 GHz as before. But in this stage, there can be large concentrations of large ice particles that would create a strong scattering signature unless the updrafts also suspend copious amounts of supercooled water to the same altitudes as the ice particles. During the dissipating stage there will be weaker 10.7 and 19.35 GHz signatures. If large ice particles are still present, there can be depressions at 85.5 GHz.

Thunderstorm Overview

Beginning on 28 August 1999, low-level convergence and support from upper levels spawned a convective outbreak throughout the Kwajalein radar range. For this study the system of interest began organizing near 0000 UTC on 29 August 1999 about 70 kilometers to the east of Kwajalein. By 0056 UTC (Fig. 2a), the line was approximately 30 kilometers to the southeast of Kwajalein. The convective band was oriented northwest to southeast and approximately 60 kilometers in length. The system moved to the southwest at eleven meters per second. By the time the DC-8 began sampling the system, short, transverse bands began forming along the southern end of the line. Cloud tops for this system reached near 15 kilometers and radar reflectivity in the stronger cells often exceeded 40 dBZ. The freezing level was approximately 5 kilometers, as observed by sounding data taken on Kwajalein.

As indicated in Figures 2-5, the radar sampled continuously and the DC-8 flew along the backside, parallel to the main convective line. Only cells in the main convective line are analyzed for this study. Other cells adjacent to, or transverse to the main line, were not within the sampling range of the radiometer aboard the DC-8. As shown in Figures 2-5, the DC-8 made several passes over the convective region as the storm system evolved.

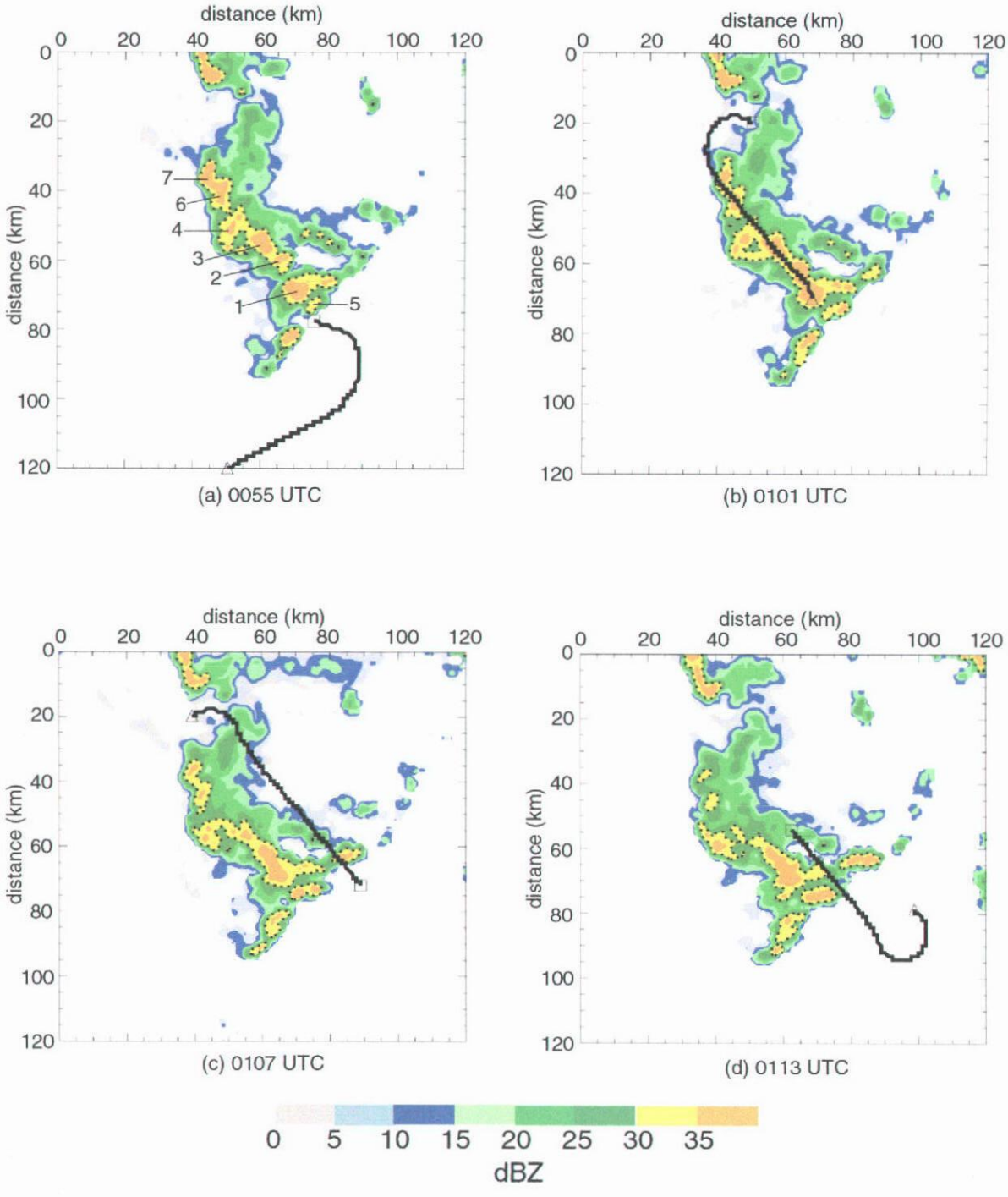

Figure 2. Radar reflectivity (dBZ) at 1 km altitude for times (a) 0055 UTC, (b) 0101 UTC, (c) 0107 UTC, and (d) 0113 UTC. The Kwajalein radar is located at the origin (0,0). Axes are labeled in distance (km) from the radar. The DC-8 flight track is overlaid in black. The cells are labeled in (a).

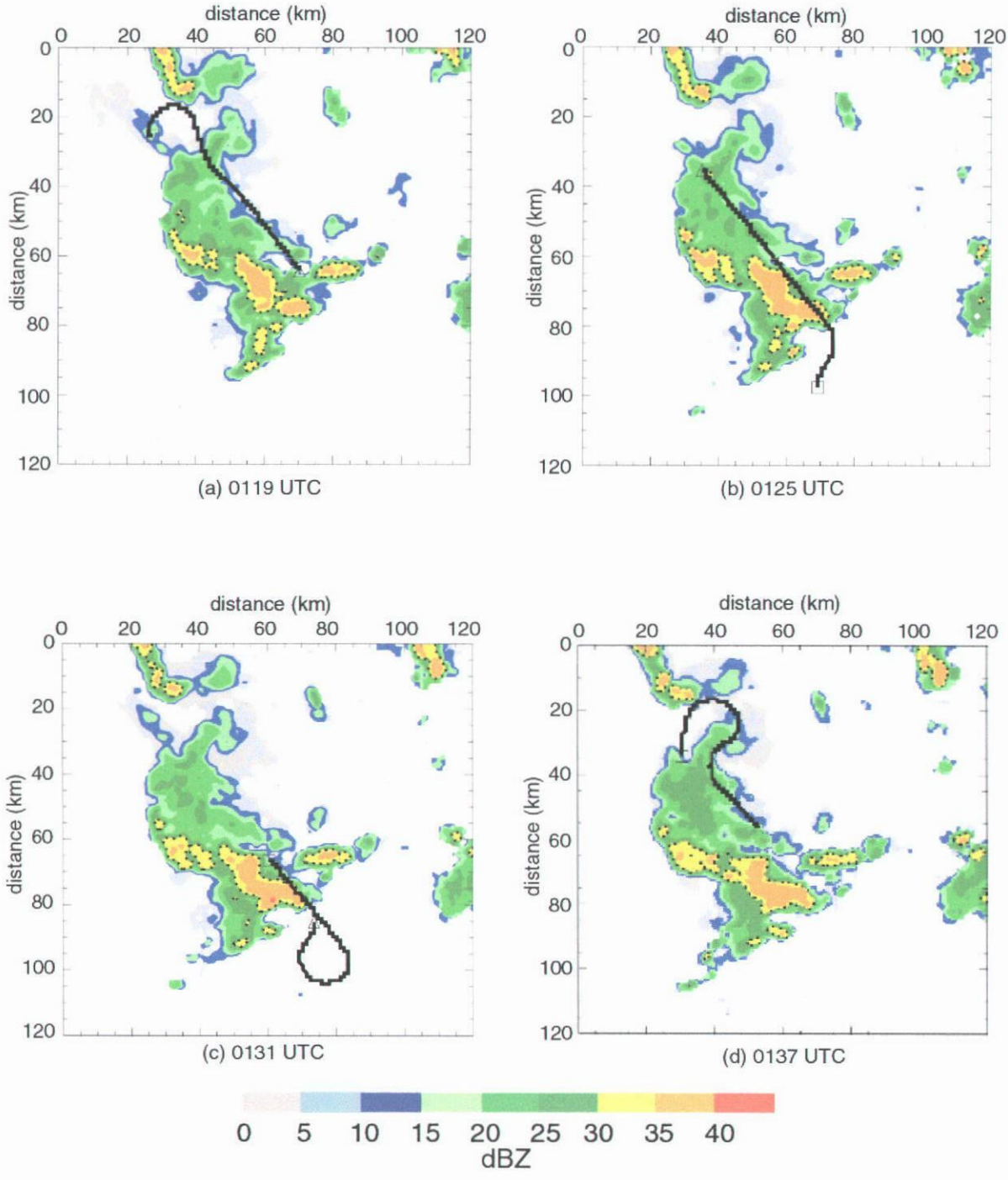

Figure 3. Radar reflectivity (dBZ) at 1 km altitude for times (a) 0119 UTC, (b) 0125 UTC, (c) 0131 UTC, and (d) 0137 UTC. The Kwajalein radar is located at the origin (0,0). Axes are labeled in distance (km) from the radar. The DC-8 flight track is overlaid in black.

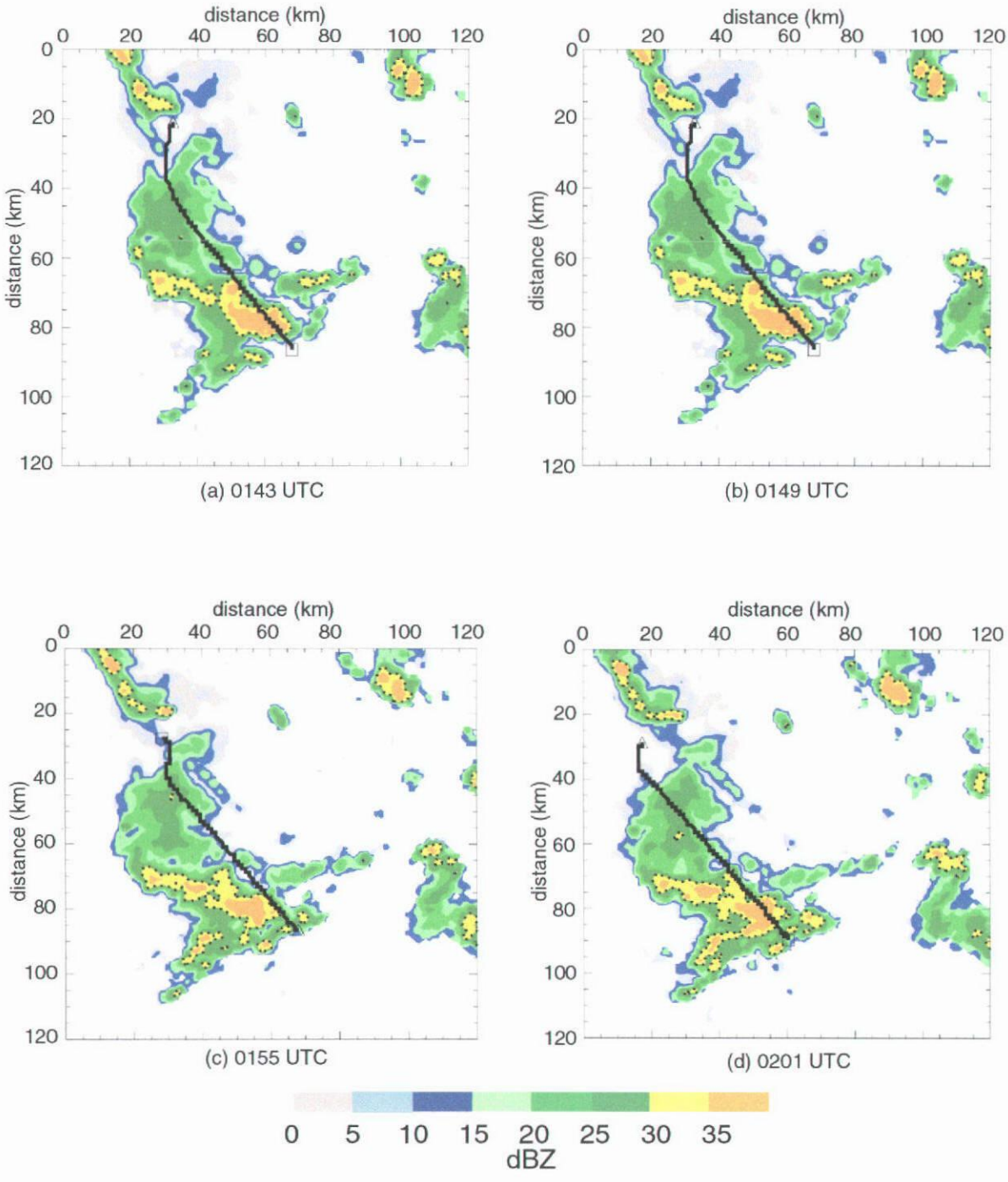

Figure 4. Radar reflectivity (dBZ) at 1 km altitude for times (a) 0143 UTC, (b) 0149 UTC, (c) 0155 UTC, and (d) 0201 UTC. The Kwajalein radar is located at the origin (0,0). Axes are labeled in distance (km) from the radar. The DC-8 flight track is overlaid in black.

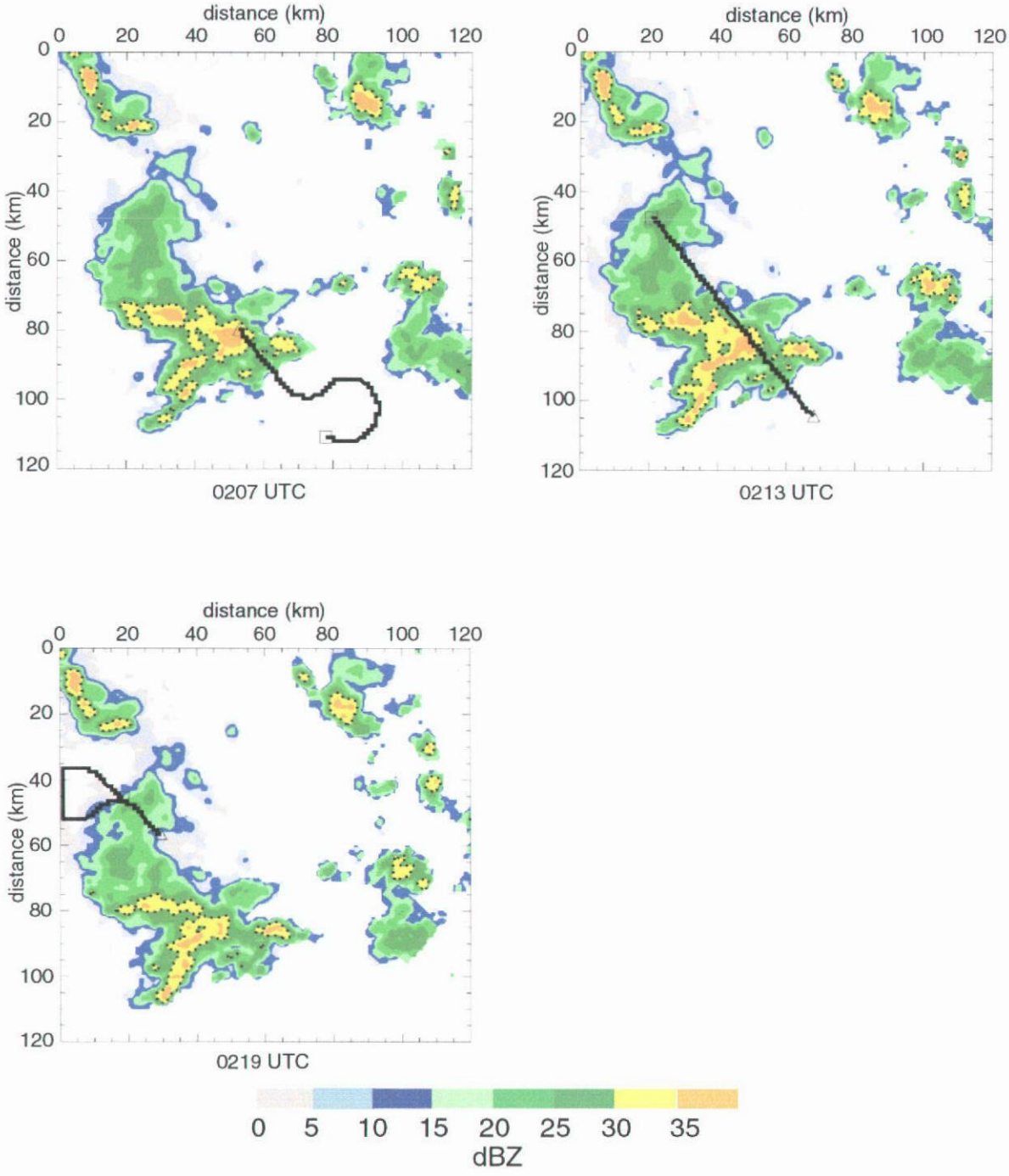

Figure 5. Radar reflectivity (dBZ) at 1 km altitude for times (a) 0207 UTC, (b) 0213 UTC, and (c) 0219 UTC. The Kwajalein radar is located at the origin (0,0). Axes are labeled in distance (km) from the radar. The DC-8 flight track is overlaid in black.

Analysis & Methods

Before analysis, the Kwajalein radar data and Advanced Microwave Precipitation Radiometer data were quality controlled. The radar data were edited using NCAR's SOLO software package (Nettleton et al. 1993) to remove spurious echo not associated with precipitation. The data from the AMPR were quality controlled by NASA's Marshall Space Flight Center before it was released and therefore required no further editing before analysis.

To analyze the radar data, it was necessary to interpolate the data from a polar coordinate system to a Cartesian coordinate system using NCAR's REORDER software package (Mohr et al. 1986). The data were interpolated to a horizontal resolution of one kilometer and a vertical resolution of 0.5 kilometers. For further analysis, NCAR's CEDRIC software package (Mohr et al. 1983) was used to create ASCII grids of the radar data.

To locate cell centers, radar reflectivity at a constant altitude of one kilometer was used. Reflectivity maximums were located in the initial volume scan at 0055 UTC and followed throughout the cell's life cycle. Brightness temperature values at all four frequencies were then collocated spatially with the low-level cell center. Because it takes approximately five to six minutes for the radar to complete a volume scan, the brightness temperature that is closest to the cell center within the volume scan period is used. For each cell identified, the vertical profile of maximum reflectivity at each level in the cell was also constructed. A time series of the vertical profiles of maximum reflectivity was

developed to illustrate the stage of the cell's life cycle and to compare with the brightness temperatures measured by AMPR.

Results

1.) Cell1 (Figure 6)

At 0055 UTC, cell 1 is in the early mature stage of a thunderstorm. High radar reflectivity, but relatively low 10 GHz brightness temperatures suggest that the precipitation is still light. The cell reaches maturity by 0119 UTC. At this time, 10 GHz brightness temperatures are at a maximum indicating heavy rainrates. Brightness temperatures at 19 and 37 GHz show a small depression, while brightness temperatures at 85 GHz show a large depression. These depressions indicate the presence of large ice which is consistent with the high reflectivity aloft. One interesting point to note is the decrease at 10 GHz and simultaneous increase in 85 GHz at 0125 UTC. Because the depression at 85 GHz was so short-lived, one possible explanation for this subsequent increase, is that supercooled liquid water is being suspended by the updraft and has not yet frozen. Supercooled liquid water within the ice layer would absorb some of the energy being scattered by the ice and re-emit it. Between 0125 and 0137 UTC, the 85 GHz temperature decreases while the 10 GHz temperature stays nearly constant. This suggests that the supercooled water may have been removed during this time. After 0137 UTC, there is a decrease in brightness temperature at all frequencies except for 85 GHz, which remains fairly steady. This would indicate that the rain layer is decreasing and the cloud is becoming totally glaciated.

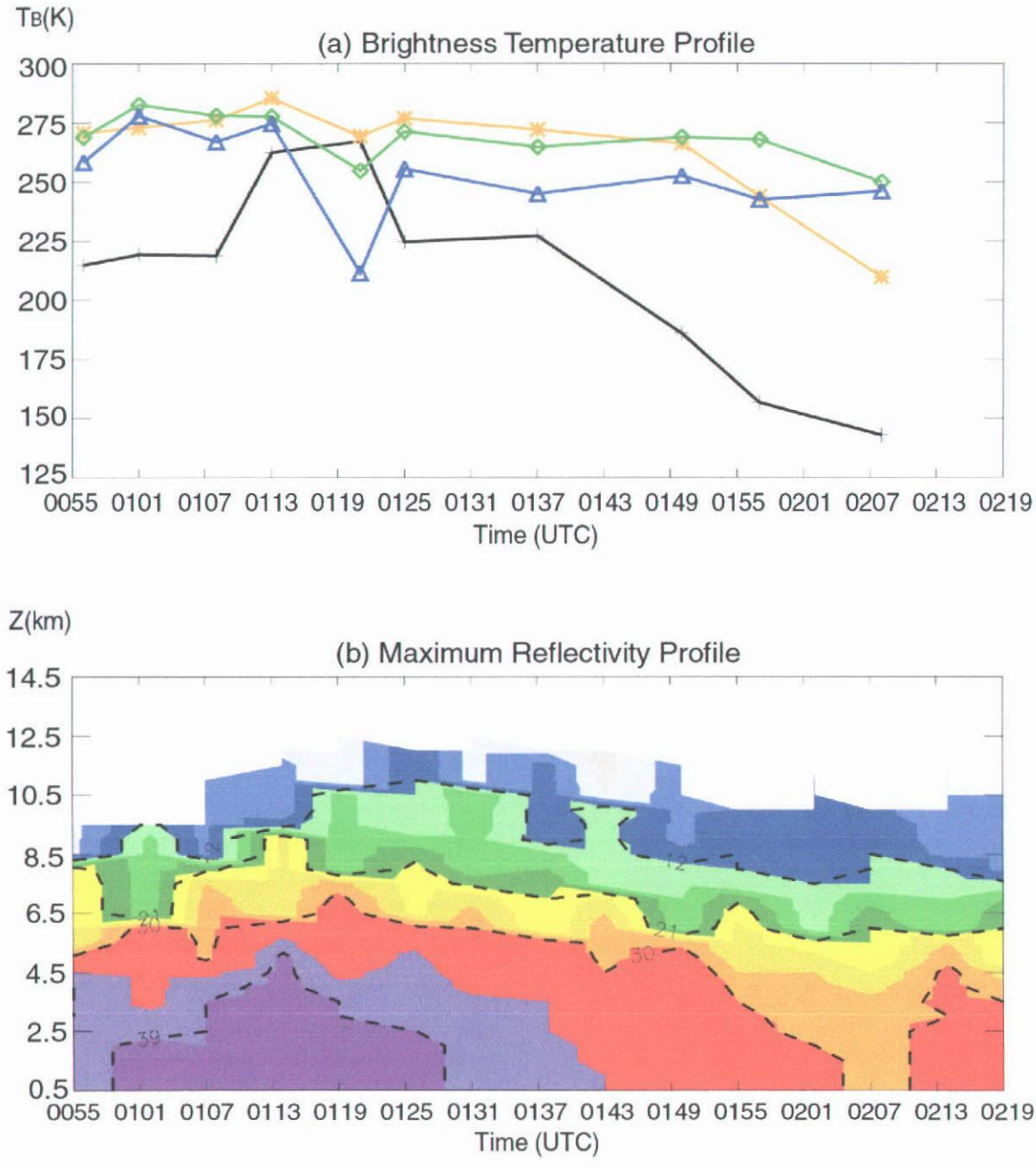

Figure 6. (a) Top graph indicates brightness temperature in Kelvin units at 10 GHz (black), 19 GHz (orange), 37 GHz (green), and 85 GHz (blue) vs. time for cell1. (b) Bottom graph depicts time-height contours of maximum reflectivity (dBZ) for cell 1.

2.) Cell 2 (Figure 7)

This cell requires less discussion because it merges with cell 1 by 0113 UTC. Only two observations were recorded by AMPR before cell 2 became indistinguishable from cell 1 due to the merger. High 37 GHz and 85 GHz brightness temperatures and moderate 10 GHz brightness temperatures, coupled with radar reflectivity data indicating moderate reflectivity and low cloud tops, show that cell 2 is in its early stages of evolution before the merger.

3.) Cell 3 (Figure 8)

Cell 3 also requires little discussion as it also merged with cell 1 by 0119 UTC. Decreasing 10 GHz and 19 GHz brightness temperatures, and 85 GHz brightness temperatures that indicate the presence of ice, show that before the merger, cell 3 has already matured and was beginning to decay. It is interesting to note the brightness temperature profiles at 0101 UTC for cell 3 and at 0155 UTC for cell 1. Both of these represent a transition from convective to stratiform cloud structure. The cold 10 GHz temperature suggests low rain rates, but the slight depression at 85 GHz is representative of some large ice particles aloft. Indeed, the reflectivities aloft are still moderately strong. Biggerstaff and Houze (1993) suggest that the low rain rates in the transition zone are the effect of deep subsidence in the cloud during this time. Subsidence would sublimate small ice crystals and decreases the amount of aggregation needed to grow large raindrops upon melting. The hypothesis of Biggerstaff and Houze (1993) is consistent with low 10 GHz temperatures and depressed 85 GHz signatures in both cell 1 and cell 3 during their dissipation stages.

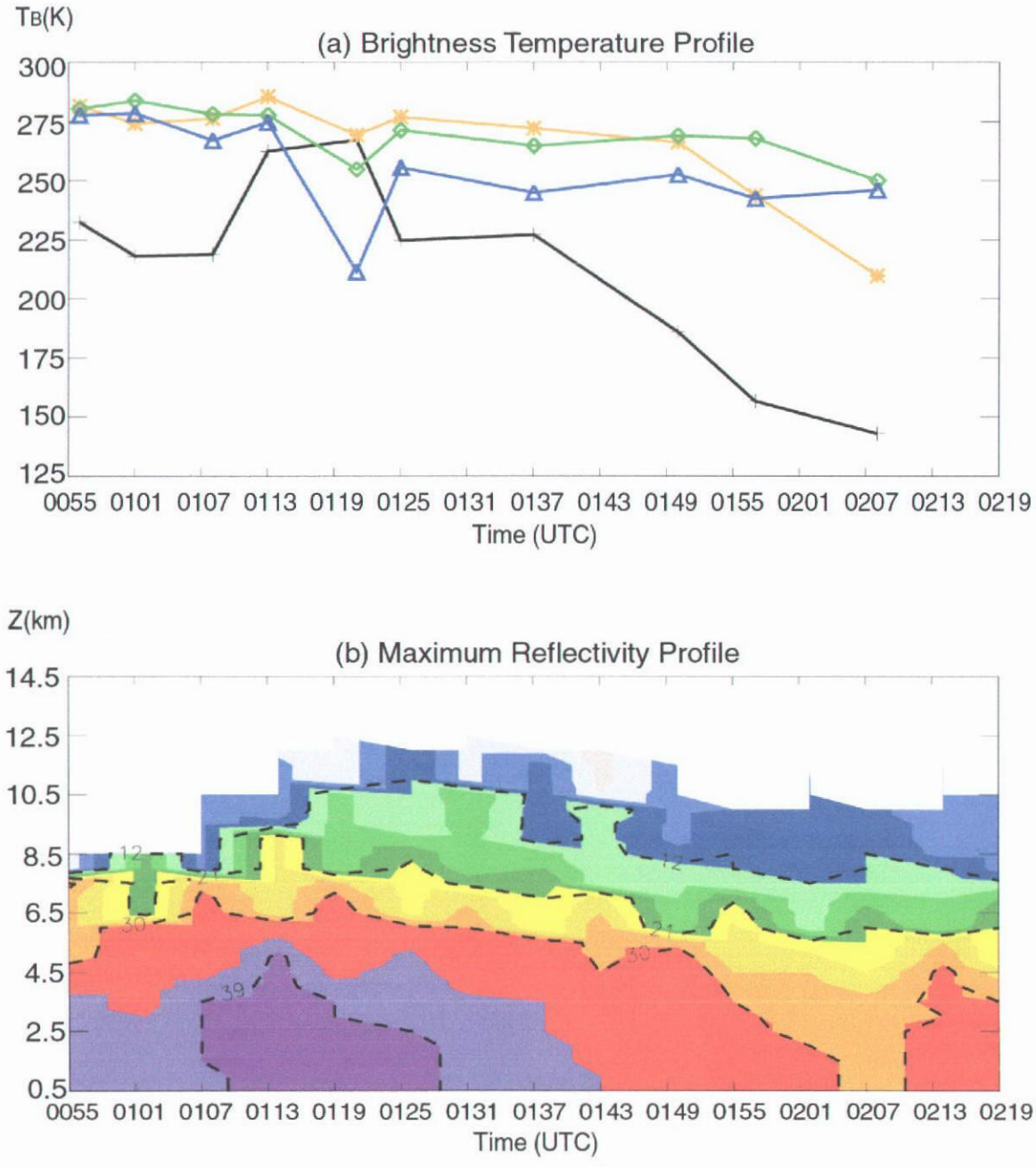

Figure 7. (a) Top graph indicates brightness temperature in Kelvin units at 10 GHz (black), 19 GHz (orange), 37 GHz (green), and 85 GHz (blue) vs. time for cell 2. (b) Bottom graph depicts time-height contours of maximum reflectivity (dBZ) for cell 2.

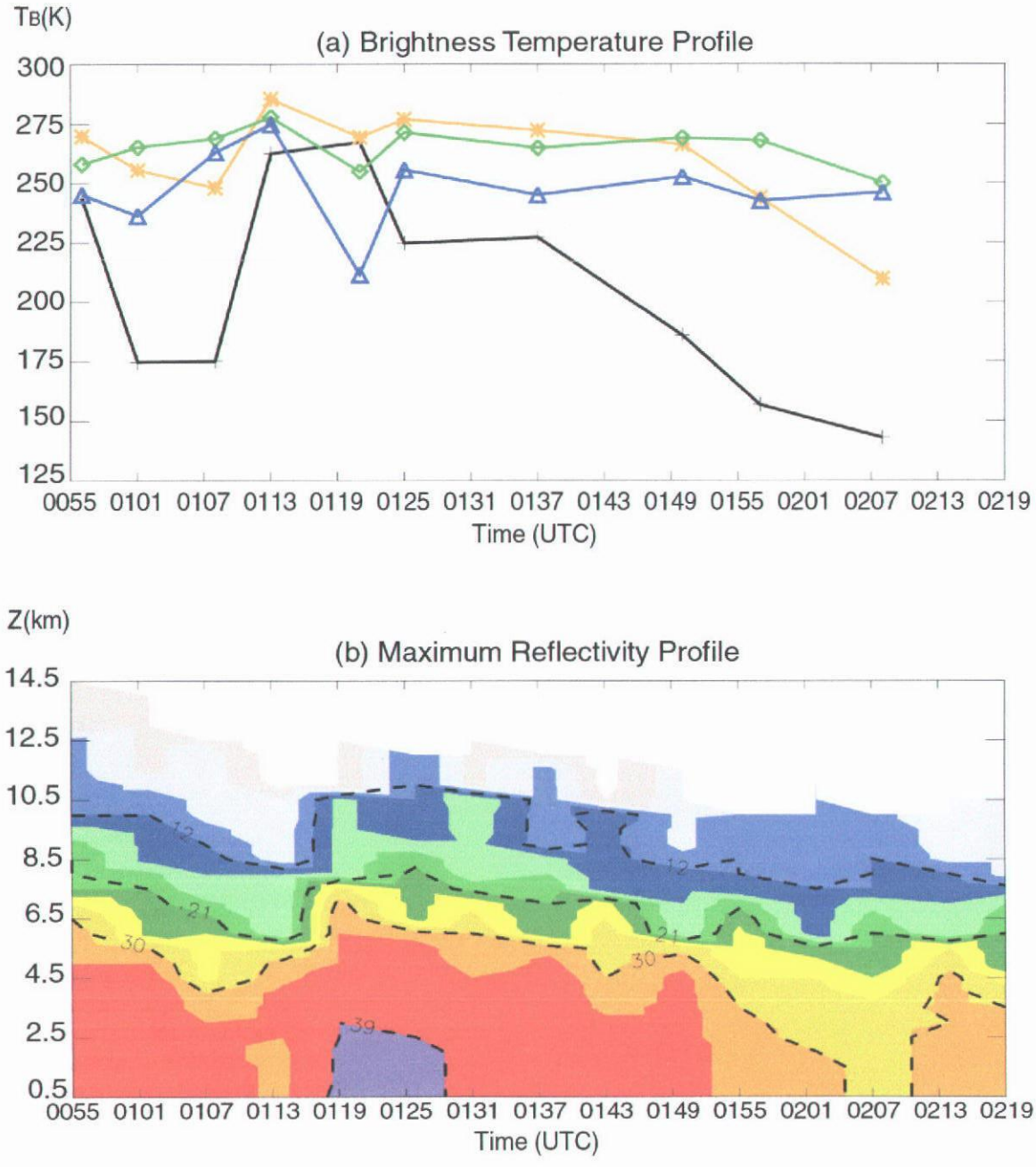

Figure 8. (a) Top graph indicates brightness temperature in Kelvin units at 10 GHz (black), 19 GHz (orange), 37 GHz (green), and 85 GHz (blue) vs. time for cell 3. (b) Bottom graph depicts time-height contours of maximum reflectivity (dBZ) for cell 3.

4.) Cell 4 (Figure 9)

This cell contains fewer brightness temperature data points than the other cells due to the fact that it often fell outside of the AMPR swath width. From both the reflectivity data and the brightness temperature data, it is evident that this cell is decaying and becoming stratiform. At the beginning of the observation period, a low rainrate is suggested by the 10 GHz brightness temperature. The 85 GHz channel observes a low brightness temperature for the implied rainrate, indicating the presence of ice. Over the next thirty minutes, 10 and 19 GHz brightness temperatures decrease, while 37 and 85 GHz brightness temperatures increase. This generally implies very little rain and very little large ice particles aloft. Surprisingly, the reflectivity remains more uniform. Since reflectivity is related to the sixth power of the particle diameters, there must still be a few large particles at all levels but not in sufficient quantities to produce high rain rates.

5.) Cell 5 (Figure 10)

Cell 5 is a very interesting case. At the beginning of the observation period, the cell is in its very early stages as indicated by both the brightness temperatures and the radar reflectivity. As the updraft becomes stronger, the reflectivities increase as well as the height of the cloud tops. A steady increase in 10 GHz brightness temperatures and a decrease in 37 and 85 GHz brightness temperatures also indicate an increase in the strength of the updraft and the production of both heavy rain and large ice particles aloft. At 0137 UTC there is a maximum at 10 GHz, as well as a depression at 37 and 85 GHz that correspond with the area of high reflectivity. Beginning at 0143 UTC, cell 5 shows an unexpected 10 GHz profile in relation to the reflectivity data and to the other channels

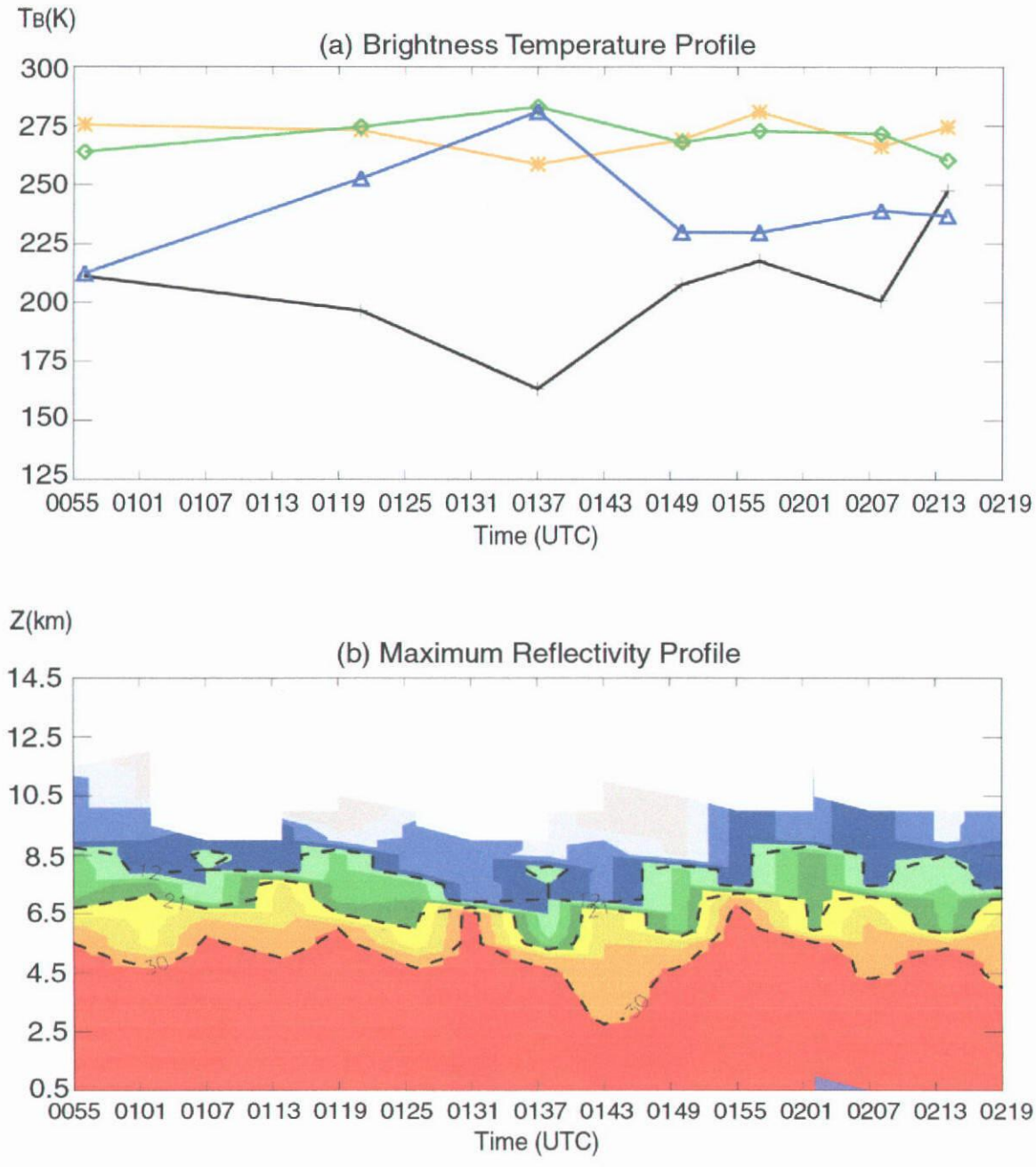

Figure 9. (a) Top graph indicates brightness temperature in Kelvin units at 10 GHz (black), 19 GHz (orange), 37 GHz (green), and 85 GHz (blue) vs. time for cell 4. (b) Bottom graph depicts time-height contours of maximum reflectivity (dBZ) for cell 4.

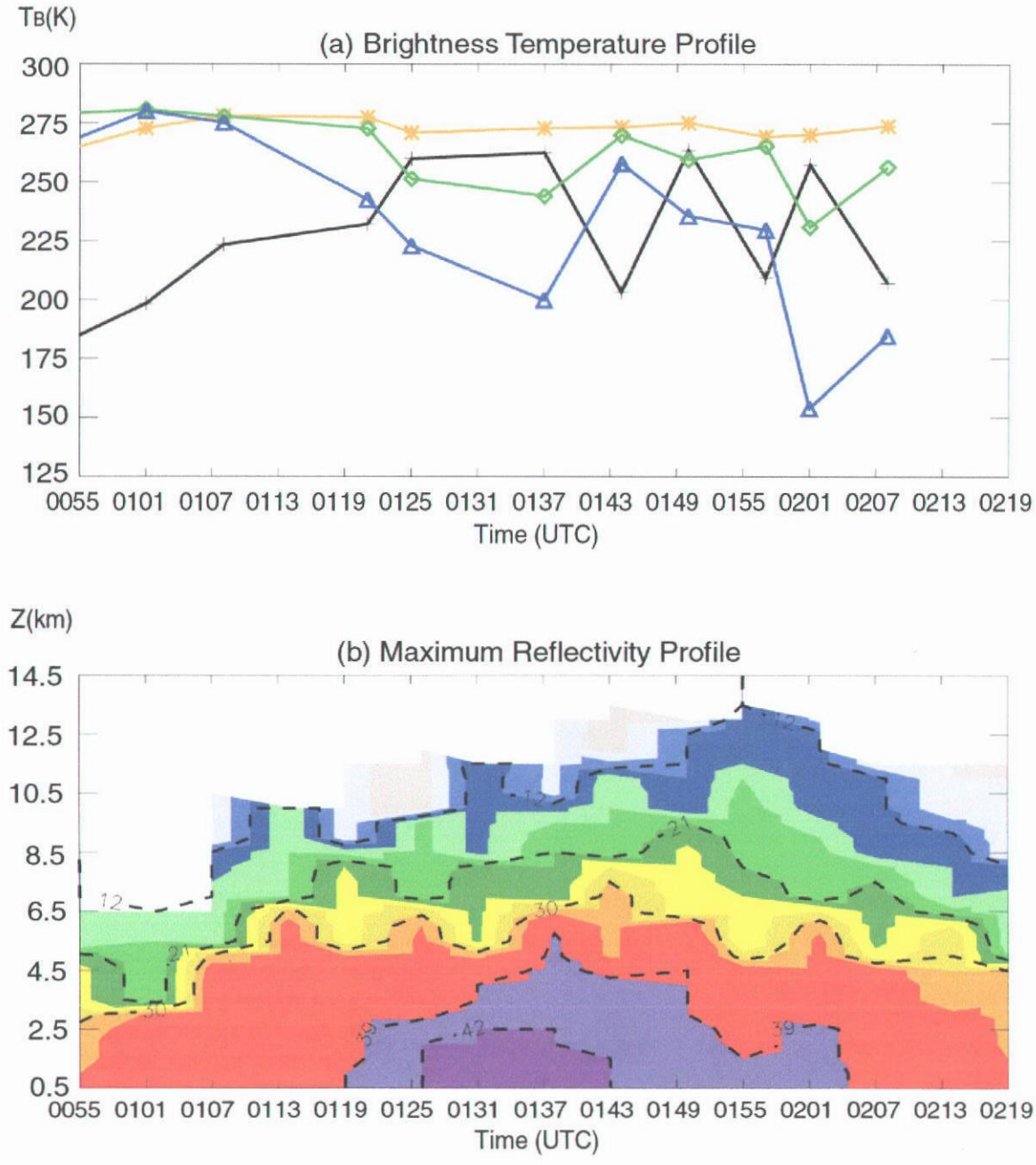

Figure 10. (a) Top graph indicates brightness temperature in Kelvin units at 10 GHz (black), 19 GHz (orange), 37 GHz (green), and 85 GHz (blue) vs. time for cell 5. (b) Bottom graph depicts time-height contours of maximum reflectivity (dBZ) for cell 5.

of the AMPR. The 10 GHz profile begins to oscillate with maxima again near 0149 UTC and 0201 UTC. As indicated in Fig. 4 and reflectivity profile in Fig. 10, the aircraft actually penetrated the convective cell rather than being able to fly over it. The turbulence encountered by the aircraft jiggled the AMPR instrument and created some uncertainty in the pointing angle during some of these passes. Given the storm structure and the physical relationship between 10 GHz and heavy rain, we believe the 0143 and 0155 UTC measurements are spurious. An interpolation in time from the remaining samples would give a more accurate view of the true 10 GHz signature.

The 37 GHz and 85 GHz brightness temperatures increase at 0143 UTC, but then begin another steady decrease until they reach their lowest values for this cell. Again, the 0143 UTC measurement is likely spurious. At 0201 UTC, the 85 GHz brightness temperatures recorded are the lowest for the entire data set. This would indicate a thick layer of large ice particles. The depression also appears strongly at 37 GHz.

6.) Cell 6 (Figure 11)

Similar to cell 4, this cell was also caught in its dissipating stage. By 0119 UTC, reflectivity values and 10 GHz brightness temperatures decrease, indicating a low rainrate. As is expected with a stratiform region, some presence of ice is indicated by the 85 GHz brightness temperatures. This is supported by evidence of the bright band in the radar reflectivity data, indicating the melting of ice.

7.) Cell 7 (Figure 12)

In cell 7 there is also evidence of the transition zone from convective to stratiform. The 10 GHz brightness temperatures decrease until about 0119 UTC

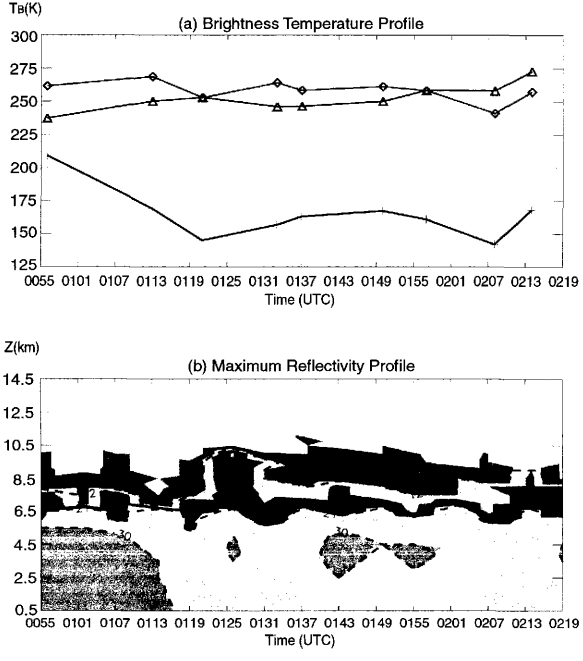

Figure 11. (a) Top graph indicates brightness temperature in Kelvin units at 10 GHz (black), 19 GHz ( ), 37 GHz (green), and 85 GHz (blue) vs. time for cell 6. (b) Bottom graph depicts time-height contours of maximum reflectivity (dBZ) for cell 6.

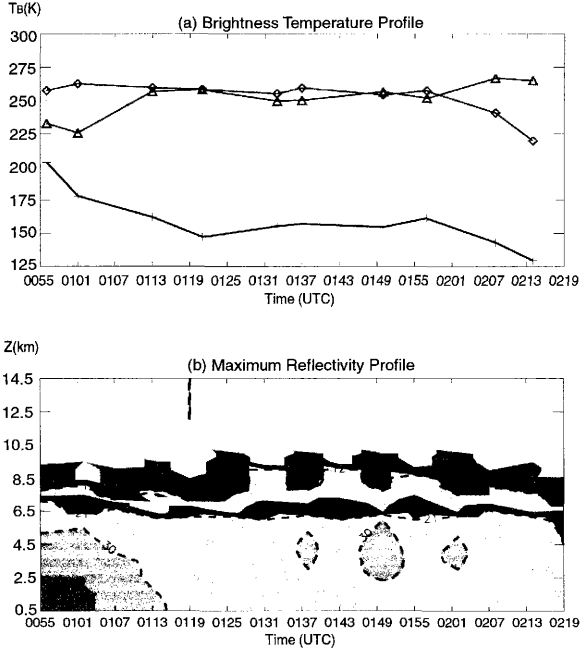

Figure 12. (a) Top graph indicates brightness temperature in Kelvin units at 10 GHz (black), 19 GHz ( ), 37 GHz (green), and 85 GHz (blue) vs. time for cell 7. (b) Bottom graph depicts time-height contours of maximum reflectivity (dBZ) for cell 7.

indicating a low rainrate. At the beginning of the observation period, the 85 GHz brightness temperatures also decrease indicating more scattering by ice. After 0119 UTC the cell becomes stratiform. Rainrates vary slightly with reflectivity as the 10 GHz brightness temperatures climb slowly between 0119 and 0155 UTC. The 85 GHz brightness temperatures increase at 0113 UTC and remain fairly steady throughout the observation period. However, there is a slight depression between 0131 and 0137 UTC associated with slightly higher reflectivity aloft.

Conclusions

Brightness temperature profiles and maximum reflectivity profiles from convective cells in the tropics were analyzed to document their relationship as a function of the life cycle of convective cells. The evolution of the 29 August 1999 storm system shows that the brightness temperature profiles can be adequately described in terms of the idealized structure of a single-cell thunderstorm based on the conceptual model of Byers and Braham (1949). During the developing stage of the thunderstorm cell, low radar reflectivity and low 10 GHz brightness temperatures, as well as high 85 GHz brightness temperatures were observed. This showed that there was little precipitation and little ice formation. During the mature stage of the cell, when reflectivity reached its maximum, the results typically showed a depression in the 37 and 85 GHz brightness temperatures due to ice scattering, and a high 10 and 19 GHz brightness temperature indicating heavy rainrates. The initial strong depression was usually short-lived, possibly denoting the presence of supercooled water above the freezing level, which tends to mask this depression in brightness temperature. One interesting feature noted several times in the results is the transition from mature to dissipating stages. In this period, 10 GHz brightness temperature were observed to decrease, indicating low rainrates, while 85 GHz brightness temperatures continued to indicate the presence of ice. This supports assertions by Biggerstaff and Houze (1993) that the processes affecting the transition zone are microphysically driven. During the dissipating stage of the cells, which was observed many times in this research, evidence of the bright band can be seen in the radar

reflectivity data. This is supported by the presence of ice as indicated by the 85 GHz signature.

The data analyzed made it possible to distinguish between liquid water, supercooled water, and ice, while allowing inferences to be made about the evolving distributions of the hydrometeors within the thunderstorm cells. As the cells matured, the changing distributions of liquid drops and ice particles were recognized. Some speculation can also be made regarding the sizes of the particles. For a example, a very strong brightness temperature depression extending from 85 GHz down to the 19 GHz channel indicated the presence of large graupel.

While the results from this data set generally followed the conceptual model, some deviations were seen. There are many factors to consider in trying to diagnose these deviations, some of which include the various microphysical processes within the cell, as well as interactions between cells within the convective system.

Because convection is so variable over different regimes and environmental conditions, it is important that the size of the data set of cases of evolution be increased. Further evolutionary cases need to be collected and analyzed before any comprehensive conclusions can be reached. This research has shown that brightness temperature and radar reflectivity data can be coupled to interpret the thunderstorm cell's stage of evolution, along with the evolution of the hydrometeors within the cell. Accurately interpreting the evolution of storm cells and storm systems is an important step in attaining TRMM's goal of describing the latent heating in the tropics.

References

Adler, R.R., and I.M. Hakkarinen, 1991: Aircraft multifrequency passive microwave observations of light precipitation over the ocean. *J. Atmos. Oceanic Technol.*, **8**, 201-220.

Biggerstaff, M.I., and R.A. Houze, Jr., 1993: Kinematics and microphysics of the transition zone of he 10-11 June 1985 squall line. *J. Atmos. Sci.*, **50**, 3091-3110.

Byers, H.R. and R.R. Braham, 1949: The Thunderstorm Project. U.S. Weather Bureau, U.S. Dept. of Commerce, Washington, D.C., 287 pp. [NTIS PB234515].

DeMaria, M., 1985: Linear response of a stratified tropical atmosphere to convective forcing. *J. Atmos. Sci.*, **42**, 1944-1959.

Hartmann, D.L., H.H. Hendon and R.A. Houze, Jr., 1984: Some implications of the mesoscale circulations in tropical cloud clusters for large-scale dynamics and climate. *J. Atmos. Sci.*, **41**, 113-121.

Houze, R.A. Jr., 1982: Cloud clusters and large-scale vertical motions in the tropics. *J. Meteorol. Soc. Japan*, **60**, 396-410.

Liu, G. and J.A. Curry, 1998: Remote sensing of ice water characteristics in tropical clouds using aircraft microwave measurements. *J. Appl. Meteor.*, **37**, 337-355.

McGaughey, G., E.J. Zipser, R.W. Spencer, and R.E. Hood, 1996: High-resolution passive microwave observations of convective systems over the tropical Pacific ocean. *J. Appl. Meteor.*, **35**, 1921-1947.

McGaughey, G. and E.J. Zipser, 1996: Passive microwave observations of the stratiform regions of two tropical oceanic mesoscale convective systems. *J. Appl. Meteor.*, **35**, 1949-1962.

Mohr, C.G. and L.J. Miller, 1983: CEDRIC - A software package for Cartesian space editing, synthesis and display of radar fields under interactive control. *Preprints, 21st Conf. On Radar Meteor.*, 19-23 September 1983, Edmonton, Alta., Canada, Publ. by Amer. Meteor. Soc., 559-574.

Mohr, C.G., L.J. Miller, R.L. Vaughan, and H. Frank, 1986: The merging of mesoscale data sets into a common Cartesian format for efficient and systematic analysis. *J. Atmos. Ocean. Tech.*, **1**, 143-161.

Nettleton, L., S.Daund, R.Neitzel, W.C. Lee, and P.H. Hildebrand, 1983: SOLO: A program to peruse and edit radar data. *Preprints, 26th Conf. On Radar Meteor.*, 1993, Norman, OK, Publ. by Amer. Meteor. Soc., 338-339.

Olson, W.S., C.D. Kummerow, Y. Hong, and W.-K. Tao, 1999: Atmospheric latent heating distributions in the tropics derived from satellite passive microwave radiometer measurements. *J. Appl. Meteor.*, **38**, 633-644.

Riehl, H. and J.S. Malkus, 1958: On the heat balance in the equatorial trough zone. *Geophysica (Helskinki)*, **6**, 503-538.

Simpson, J., R.F. Adler, and G.R. North, 1988: A proposed Tropical Rainfall Measuring Mission (TRMM) satellite. *Bull. Amer. Met. Soc.*, **69**, 278-295.

Smith, E.A., A. Mugani, H.J. Cooper, G.J. Tripoli, and X. Xiang, 1992: Foundations for statistical-physical precipitation retrieval from passive microwave satellite measurements. Part I: Brightness-temperature properties of a time-dependent cloud radiation model. *J. Appl. Meteor.*, **31**, 506-531.

Spencer, R.W., R.E. Hood, F.J. La Fontaine, E.A. Smith, R. Platt, J. Galliano, V.L. Griffin, and E. Lobl, 1994: High-resolution imaging of rain systems with the Advance Microwave Precipitation Radiometer. *J. Atmos. Oceanic Technol.*, **11**, 849-857.

Viltard, N., E. Obligis, V. Marecal, and C. Klapisz, 1998: Retrieval of precipitation from microwave airborne sensors during TOGA COARE. *J. Appl. Meteor.*, **37**, 701-717.

Weisman, M.L. and J.B. Klemp, 1986: *Characteristics of Isolated Convective Storms.* Chap. 15 in Mesoscale Meteorology and Forecasting, edited by P.S. Ray, Amer. Meteor. Soc., 793 pp.

Wilheit, T.T., A.T.C. Chang, M.S.V. Rao, E.B. Rodgers, and J.S. Theon, 1977: A satellite technique for quantitatively mapping rainfall rates over the oceans. *J. Appl. Meteor.*, **16**, 551-560.

Wilheit, T.T., A.T.C. Chang, J.L. King, E.B. Rodgers, R.A. Nieman, B.M. Krupp, A.S. Milman, J.S. Stratigos, and H. Siddalingaiah, 1982: Microwave radiometric observations near 19.35, 92, and 183 GHz of precipitation in tropical storm Cora. *J. Appl. Meteor.*, **21**, 1137-1145.

Wilheit, T.T., 1986: Some comments on passive microwave measurement of rain. *Bull. Amer. Met. Soc.*, **67**, 1226-1232.

Yanai, M., S. Esbensen, and J. Chu, 1973: Determination of bulk properties of tropical cloud clusters from large-scale heat and moisture budgets. *J. Atmos. Sci.*, **30**, 611-627.

CURRICULUM VITAE

ANITA DENISE RAPP
April 2000

Education

Candidate for B.S., Texas A&M University, Meteorology, May 2000.

Professional Experience

1999-2000 President, Texas A&M Student Chapter of the American Meteorological Society.

1998-1999 Secretary, Texas A&M Student Chapter of the American Meteorological Society.

1998-present Mesoscale Research Group Student Technician.

Field Program Experience

1999 Assistant scientist for the Kwajalein Experiment (KWAJEX) based in the Republic of Marshall Islands.

1998 Radar operator for the Texas-Florida Underflight (TEFLUN-A) experiment based in College Station, TX.

Honors

1999-2000 University Undergraduate Research Fellow

1998-2000 Academic Incentive Award

1996-2000 Distinguished Student

1996-2000 Dean's Honor Roll

Professional Memberships

American Meteorological Society
Golden Key National Honor Society
Sigma Xi Research Honor Society
Phi Eta Sigma National Honor Society